

# The role of niobium in improving toughness and corrosion resistance of high speed steel laser hardfacings

Manel Rodríguez Ripoll<sup>1\*</sup>, Niko Ojala<sup>2</sup>, Christian Katsich<sup>1</sup>,  
Vladimir Totolin<sup>1</sup>, Christian Tomastik<sup>1</sup>, Klaudia Hradil<sup>3</sup>

<sup>1</sup>*AC2T research GmbH, Viktor-Kaplan-Straße 2/C, 2700 Wiener Neustadt, Austria.*

<sup>2</sup>*Tampere University of Technology, Department of Material Science, Tampere Wear Center,  
P.O. Box 589, 33101 Tampere, Finland.*

<sup>3</sup>*Technische Universität Wien, X-ray centre, Getreidemarkt 9, 1060 Vienna, Austria.*

Hardfacing by laser provides a cost-effective option for protecting components against mechanical wear and corrosion. In the present work, high speed steel hardfacings were deposited using a high-power direct diode laser with the aim of investigating the role of niobium content on their mechanical and corrosion properties. The content of niobium was varied between 0.1 and 3 wt.%. The results show that niobium content has a high impact on the hardfacing microstructure and its resulting mechanical properties. In particular, niobium is able to significantly enhance the abrasive wear resistance of high speed steel laser hardfacings. This improvement is accompanied by a superior corrosion resistance. The impact of niobium content on slurry erosion resistance is less remarkable and a clear benefit can only be achieved by microalloying. These results are correlated with the microstructural changes induced by the varying niobium content. An increase in niobium content reduces the amount of carbides found along the grain boundaries, raises the amount of chromium dissolved in the iron matrix and increases the elastic strain to failure of the hardfacing. This results as a consequence in high speed steel laser hardfacings with superior toughness and enhanced corrosion resistance.

**Keywords:** High speed steel; Niobium; Wear; Toughness; Corrosion.

\*Corresponding author: Manel Rodríguez Ripoll: Tel. +43 2622 816 00 -309, Fax +43 2622 816 00 -99, (ripoll@ac2t.at).

# 1. INTRODUCTION

The use of components in highly demanding applications requires the design of new materials that are able to fulfil the increasing demands in terms of high strength, toughness and wear resistance while simultaneously providing an adequate corrosion protection. For instance, cutting tools undergo continuous pressure to operate at higher speeds with better accuracy and longer lifetime. Combined with the continuous increase in using difficult-to-machine materials, such as titanium and nickel alloys, these demands are driving the design of novel materials which are able to cope with these challenges. However, in many demanding applications such as mining, dredging, tunnelling or in agricultural equipment, the size of the used components limits the use of these novel materials due to economic constraints and their application is often restricted to the form of thick coatings, commonly named claddings or hardfacings. Hardfacings provide a cost-effective solution to increase wear and corrosion resistance of components operating under aggressive environments [1–11].

Among the different methods available for depositing hardfacings, hardfacing by laser has become one of the most efficient techniques thanks to its high deposition rate and efficiency. In comparison with other hardfacing technologies that rely on punctual heating sources, such as arc welding and plasma transfer arc [1–6], or conventional CO<sub>2</sub> or Nd/YAG lasers [7–9], the laser beam created by diode lasers has an elliptical shape, which increases throughput, reduces substrate dilution and avoids overheating at the turning points of the beam [10,11]. By using laser hardfacing, metal powder can be welded on the top surface of inexpensive components to enhance its operational performance. The materials typically used for hardfacings are iron, nickel and cobalt alloys, although iron is preferable for being inexpensive and environmentally friendly. Wear resistant iron-based hardfacings are usually formed by an iron matrix reinforced by the presence of carbides. Iron-based hardfacings have a very high hardness but often lack sufficient fracture toughness that could substantially improve the component service lifetime. In order to increase fracture toughness, doping elements such as niobium were recently successfully added in nickel-based laser hardfacings [7,8].

The advantages of niobium as alloying element have been known for long. Niobium has a high affinity for carbon, an unfavorable size factor and remains as independent phase providing potential nucleation sites. It also forms carbides at very high temperatures (> 3000 °C) [8,12,13]. Besides a higher wear resistance, the main advantage of having large amounts of niobium carbides is that most of the chromium remains in the metal matrix dissolve, making the steel more resistant to corrosion [12]. The role of chemical composition on hardness, wear and corrosion resistance was evaluated by Theisen et al. for several wear resistant iron-based alloys including tool steels, casting alloys and a hardfacing using several annealing temperatures [13]. The niobium content of all the investigated materials was around 5 to 6 wt.%. The authors reported that alloys containing primary niobium carbides had a good resistance to abrasion wear. In addition, the higher affinity of niobium

for carbon suppressed the formation of chromium carbides, leaving high amounts of chromium available for corrosion protection. This work opened the door to the development of wear-resistant stainless steels with higher hardness.

The use of niobium as alloying element for microstructural design of nickel-based hardfacing has been recently investigated [7,8]. The main aim was the development of hard yet tough materials by exploiting the ability of niobium to form monocarbides and inhibit grain growing by pinning grain boundaries. The main contribution of this work was the identification of the properties that an alloying element requires to successfully refine the microstructure of hardfacings in-situ during solidification. The main criterion to select the refining element was to have a higher affinity with both C and B (i.e. Gibbs free energy more negative than for Cr). However, this condition was insufficient, since a lack of refinement in Ni-based alloys was found using Zr as alloying element and had been previously observed for V, Ti, Ta, despite all these elements having a higher affinity for C than Cr. A limited solubility of the carbides in their Cr-rich counterparts was also found to be required. Further, the refining element should form carbides at higher temperatures in comparison with Cr-rich precipitates. Based on this approach, the authors showed that nickel hardfacings containing 4 wt.% Nb were able to keep the hardness of the original nickel-based alloy, despite the increase in toughness due to their finer microstructure.

The role of Nb content on the solidification process, microstructure and the resulting impact on wear resistance and fracture toughness has been systematically researched in hypereutectic high chromium cast irons [14–16]. Besides the presence of niobium monocarbides within the matrix, the addition of Nb contents up to 1.5 wt.% was reported to refine the size of  $M_7C_3$  chromium carbides, which additionally became more isotropic [14]. This behavior has been recently confirmed for Nb concentrations up to 3 wt.%. Niobium was found to substantially modify the microstructure by refining the dendrite size and by causing a partial replacement of  $M_7C_3$  chromium carbides by niobium monocarbides. Niobium monocarbides have a higher melting point and hardness than most of other carbides. This improvement in the microstructure resulted in an increase in hardness, wear resistance and fracture toughness [15]. Similar observations to those obtained for bulk materials were made on a plasma cladding iron-based alloy with a similar composition [16]. When doped with 1.5 wt.% Nb, the plasma cladding increases its wear resistance and lowers friction during ball-on-disc experiments. The improvements of the tribological properties were attributed to Nb induced changes in the cladding microstructure. Without Nb the cladding had a dendritic matrix structure typical of fast solidification processes, while the Nb-doped sample had equiaxed grains. In FeCrNbC hardfacings deposited by arc welding with higher Nb content, Scandella and Scandella noticed a reduction of abrasive wear by a factor two for samples containing 8% Nb compared to lower alloyed samples with 3% Nb [17]. The microstructure of the samples with 8% Nb was formed mainly by large niobium monocarbides surrounded by a martensitic matrix, reinforced by finer niobium carbides.

The influence of Nb on the mechanical and chemical properties of high-speed steels (HSS) has received much less attention so far. Recently Wang et al. [18] investigated the influence of 1.95 wt.% Nb content on M3 high speed steel in as-quenched state and after several heat treatments. The results showed that Nb promotes the formation of primary monocarbides and is able to pin the grain boundaries consequently reducing the grain size considerably. The addition of niobium to high speed steel tools was also investigated in concentrations of up to 0.5% as a partial substitution of vanadium [19]. Again the formation of niobium monocarbides was observed. The inclusion of niobium as alloying element did not impede the formation of secondary vanadium carbide precipitates, so that hardness was not hampered.

These previous works highlight that the role of niobium as alloying element in high speed steels has been seldom researched. Hence, a systematic investigation on the impact of Nb concentration on the mechanical and corrosion properties of high speed steels is lacking, especially in case of hardfacings. Therefore, the aim of this work is to shed light on the role of Nb as alloying element on the abrasion, erosion and corrosion properties of laser hardfacings using Nb concentrations up to 3 wt.%.

## 2. METHOD

### 2.1. Sample preparation

Commercial high speed steel powder (EuTroLoy 16606 Castolin Eutectic, Austria) was used as reference material for the hardfacings. This alloy is suitable for welding depositions and is characterised by an excellent wear resistance. The nominal chemical composition is shown in Table 1. The selected high speed steel powder was doped using niobium powder (Goodfellow, United Kingdom) with a maximum particle size of 74  $\mu\text{m}$  and purity of 99.85%.

**Table 1.** Chemical composition (weight %) of the high speed steel powder used for the hardfacings.

C	Cr	Mo	W	V	Fe
1.0	4.2	5.0	6.4	2.0	balance

The powders were mixed using polyethylene glycol dodecyl ether (Sigma Aldrich, USA) as binder until forming a homogeneous suspension. A set of samples was prepared by mixing only the high speed steel powder with the binder. These samples are denoted as reference. The other set of samples was doped with pure niobium powder using the following concentrations: 0.1, 1 and 3 wt.%. The suspension was deposited on 1.0038 mild steel plates with a dimension of 200x150x8 mm. The plates had a hardness of 150 HV30 and were ground before the deposition process. The 2 mm thick suspension was dried in a chamber furnace under ambient air for 60 min at 150 °C. Afterwards, the laser melting process of the dried suspension was performed using a

Coherent Direct Diode Laser System 8000D (Coherent, USA) (Fig. 1a). The optical lens system was set for a large melting area using a 24 mm long and 6 mm wide beam in order to provide a smooth energy transfer into the powder precursor. Powder melting speed was determined by the laser beam velocity, which was set to 3.5 mm/s with a laser energy of 4.5 kW, which results in an energy input per unit length of 1.3 kJ/mm. Argon was used as shielding gas with a flow rate of 40 l/min. After deposition on the steel substrate, the hardfacings were ground in order to obtain a well-defined plane and parallel initial surface for the wear tests. The final thickness of the hardfacings was about 1 mm.

## 2.2. Microstructure Characterisation

Cross-sections of samples were prepared in order to investigate the microstructure of as-deposited hardfacings. The sample cross-sections were ground using 2000 grit paper and polished with 3 and 1  $\mu\text{m}$  diamond paste. Afterwards, the samples were etched with 4 % nital reagent. An initial microstructure characterisation was performed using an optical microscope equipped with a digital camera (MEF4A, Leica Microsystems, Germany). Afterwards, the cross-sections were investigated at a higher resolution using scanning electron microscopy analyses. The analyses were performed using a JEOL JSM-T330A (JEOL Ltd., Japan), equipped with a light-element Si energy-dispersive X-ray detector (beryllium-window type EDX; Oxford Inst., UK). The SEM was operated using secondary and backscattered electrons at an accelerating voltage of 20 kV. Selected SEM micrographs were investigated using the image processing and analysis Leica QWin software (Leica Microsystems, Germany) for obtaining quantitative data on the microstructure of the niobium doped hardfacings. EDX maps were obtained with a Field Emission Scanning Electron Microscope equipped with a Gemini column ( $\Sigma$ igma HDPV, Zeiss, Germany) using an accelerating voltage of 20 kV.

Phase composition was analysed using x-ray diffraction investigations. The X-ray diffraction measurements were performed using a PANalytical X'Pert Pro MPD diffractometer (PANalytical B.V., The Netherlands) in Bragg-Brentano geometry. A 0.04 rad. Soller collimator and automatic divergence slits defined the beam divergency. Measurements were performed in a  $2\theta$  range from 5 to  $135^\circ$  in increments of  $0.01^\circ$  using copper  $K_{\alpha 1/2}$  radiation. The samples were placed inside a 200  $\mu\text{m}$  deep hole with 12 mm diameter of silicon single crystalline plates (orientation (711)). The working distance between sample and the X'Celerator detector was set to 240 mm. The obtained diffraction reflections were matched by comparison with the "Power Diffraction Database" PDF-4+ of the International Centre for Diffraction Data (Philadelphia, USA) included within the HighScore software suite of the PANalytical company [20].

Hardness of the as-deposited hardfacings was measured using Vickers indentation with a load of 30 kpf (HV30). Each hardness value was obtained as the average of five individual measurements. Local hardness values of the iron matrix were obtained by using nanoindentation measurements. Nanoindentation was performed using a Hysitron Triboindenter TI900 (Minneapolis, USA)

equipped with a diamond Berkovich indentation tip with 100 nm tip radius. The load cycle comprised linear loading for 5 s until reaching the applied peak load of 10 mN and a subsequent linear unloading for additional 5 s. Hardness and reduced elastic modulus were obtained from the load vs. depth curves following the procedure described by Oliver and Pharr [21]. Each value was the average of ten individual measurements.

### 2.3. Wear and Corrosion tests

Low stress abrasion resistance of the deposited hardfacings was investigated using three body abrasion tests, carried out according to ASTM-G65 standard (Fig. 1b). The ground hardfacing samples were loaded with 130 N normal load against a rubber wheel with a shore hardness of A60. Ottawa silica sand with a particles size of 212-300  $\mu\text{m}$  was fed at 340 g/min between the rubber wheel and the sample. The speed of the rubber wheel was set to 200 rpm. The total test duration was 600 s, which corresponds to a total sliding distance of 1436 m. After the tests, wear was measured using gravimetric measurements according to the standard. The surface topography of selected samples was measured using an InfiniteFocus optical 3D profilometer (Alicona, Austria).

High stress slurry erosion was evaluated using a high speed slurry-pot erosion wear tester (Tampere Wear Center, Finland) [22] presented in Fig. 1c. In this study, granite gravel with a particle size of 8-10 mm was used as abrasives with a slurry concentration of 20 wt.%. Plate samples with dimensions 64 x 40 x 12 mm were immersed in a pot containing the slurry. During the tests two of the test samples were located at the lowest sample holder level (i.e. closer to the pot bottom) while the other two samples were placed a level higher. Sample rotation was performed during the tests [22]. This means that the position of the samples was changed, so that in every test all four samples were tested on both sample levels. This ensures that, at the end of the test, the wear conditions are similar for all four specimens. The total testing time was set to 40 minutes. Every 10 minutes the samples were weighted and repositioned to new testing levels and the slurry was replaced. The rotational speed of the main shaft was 2000 rpm which corresponds to a sample tip speed of 20 m/s. The granite used originated from Sorila quarry (Tampere, Finland). Hardness of the granite was around 800 HV and the solid density 2.65 t/m<sup>3</sup>. The nominal mineral composition was plagioclase (45 %), quartz (25 %), orthoclase (13 %), biotite (10 %) and amphibole (5 %) [23].

The corrosion tests were performed with a VersaSTAT 3F potentiostat from Ametek, Inc. (Berwyn, PA USA) using an electrochemical cell with three electrode configuration. The samples were fully immersed in an electrolytic solution containing 0.5 M sulphuric acid. The high speed steel hardfacing was set to be the working electrode. The counter electrode was a 99.99% platinum wire (Goodfellow, United Kingdom) and the reference electrode was Ag/AgCl in 3M NaCl saturated solution. All potentials mentioned in the present work were referenced versus Ag/AgCl potential. The polarisation curves were obtained using a scan rate of 1 mV/s in a range between -1.2 and 1.2 V. At the beginning of the tests, a cathodic cleaning of the samples at -1.2 V for 5 minutes took

place. Afterwards, the samples were left at open circuit potential for 60 minutes for stabilisation of the equilibrium potential.

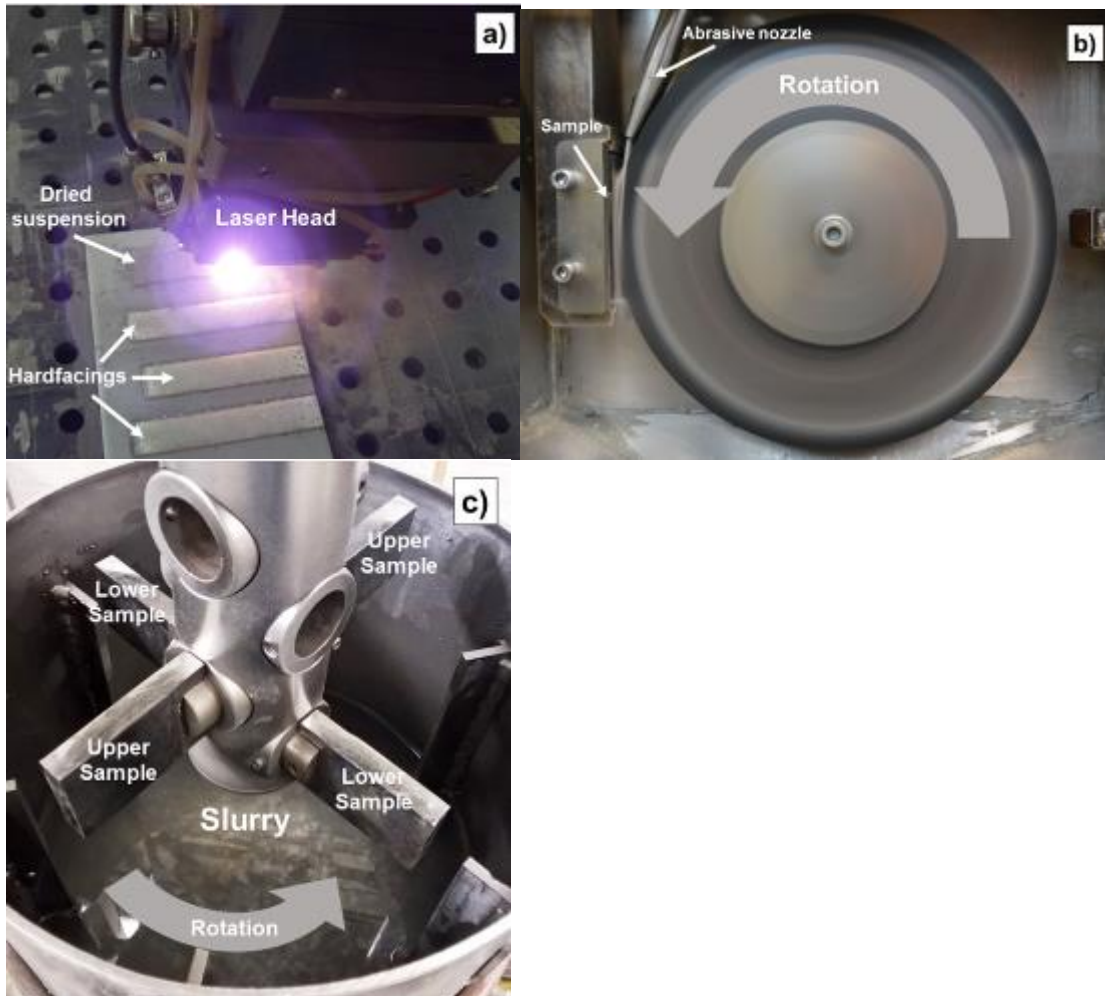


**Figure 1.** Direct Diode Laser System used for depositing the high speed steel hardfacings (a). Abrasion test rig according to ASTM G65 (b). Slurry-pot test configuration for the erosion tests. Before the test, samples are lowered to the bottom of the pot (c).

### 3. RESULTS

#### 3.1 Influence of niobium content on microstructure

The microstructures of the etched HSS hardfacings with Nb contents up to 1 wt.% show under scanning electron microscopy the presence of dendritic martensitic grains surrounded by networks of carbides (Fig. 2). Only samples containing 3 wt.% Nb show the presence of a different carbide structure. In this case, carbide networks are not only found surrounding the martensitic dendritic structures but also seem to build carbide branches running through the grains. The typical size of the dendritic grains seems to be substantially smaller, when compared to hardfacings with smaller niobium contents. Energy dispersive X-ray spectroscopy (EDX) measurements of the matrix

material in the reference hardfacing (Fig. 2a) reveal the presence of the nominal alloying elements. Carbide forming elements, W, Mo, Cr and V can be found dissolved in the matrix. The intergranular carbide network surrounding the dendrites is formed by mixed carbides with high W and Mo content (15-18 wt.%) and a concentration of Cr and V of about 5 wt.%. Their lamellar structure, bright appearance in the SEM images and the presence of mainly W and Mo suggest a dominant  $M_6C$  stoichiometry with the added presence of metastable acicular  $M_2C$  carbides (Fig. 2a) [24–26]. Cr-rich  $M_7C_3$  carbides could not be found by EDX.

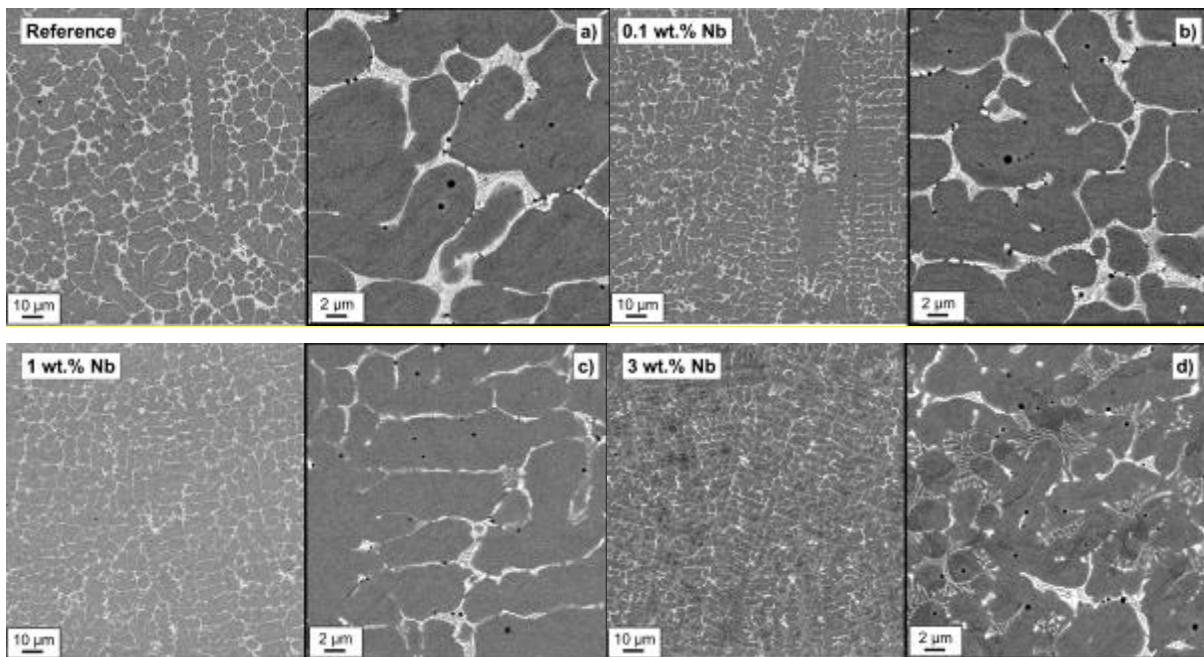


**Figure 2:** Scanning electron microscope images of the HSS laser hardfacings. Reference hardfacing (a), 0.1 (b), 1 (c) and 3 wt.% Nb (d).

Hardfacings doped with 0.1 wt.% of niobium have a very similar microstructure (Fig. 2b). The elemental composition of the matrix is very similar to the reference sample. Nb was not present in most of the spot measurements, and in a single spot could be measured with a concentration of 0.4 wt.%. The major difference respect to the reference hardfacing is that a small amount, typically about 1.5 wt.% Nb is detected in the W-Mo rich  $M_6C$  and  $M_2C$  carbides. For 1 wt.% Nb, the microstructure looks apparently similar (Fig. 2c). The dendrites have a similar composition as the previous samples. Nb is rarely found and always with a concentration smaller than 1 wt.%. The networks of  $M_6C$  and  $M_2C$  carbides surrounding the martensitic dendrites are much thinner so that the lamellar structure is much less evident, when compared to the reference material. EDX mapping reveals the presence of Mo, W and Cr in the lamellar carbides (Fig. 3). Nb enrichment is determined to occur in carbides with a paler colour and no lamellar structure, close to the dendritic structure. Besides Nb, these carbides are also Mo and V rich. No isolated Nb carbides could be found.

The microstructure changes dramatically when the niobium content increases to 3 wt.% (Fig. 2d). The carbide networks branch through the matrix forming a palm-like structure and the dendritic arm



spacing is significantly smaller. The palm structures that start in the intergranular carbide network and branch towards the grain typically have a much higher Nb content (over 10 wt.%). Additionally, isolated Nb rich (up to 30 wt.%) carbides, probably monocarbides, are found scattered in the microstructure. Nb is not always measured in the matrix and when found the concentrations rarely exceed 1 wt.%. The EDX mapping confirms the spot measurements. The presence of Mo rich carbides with W, V and Cr decreases at expenses of the palm-like Nb rich carbides with smaller content of Mo and V. This indicates that for higher Nb contents, a larger concentration of W and Cr has to remain in dissolve in the iron dendrites.

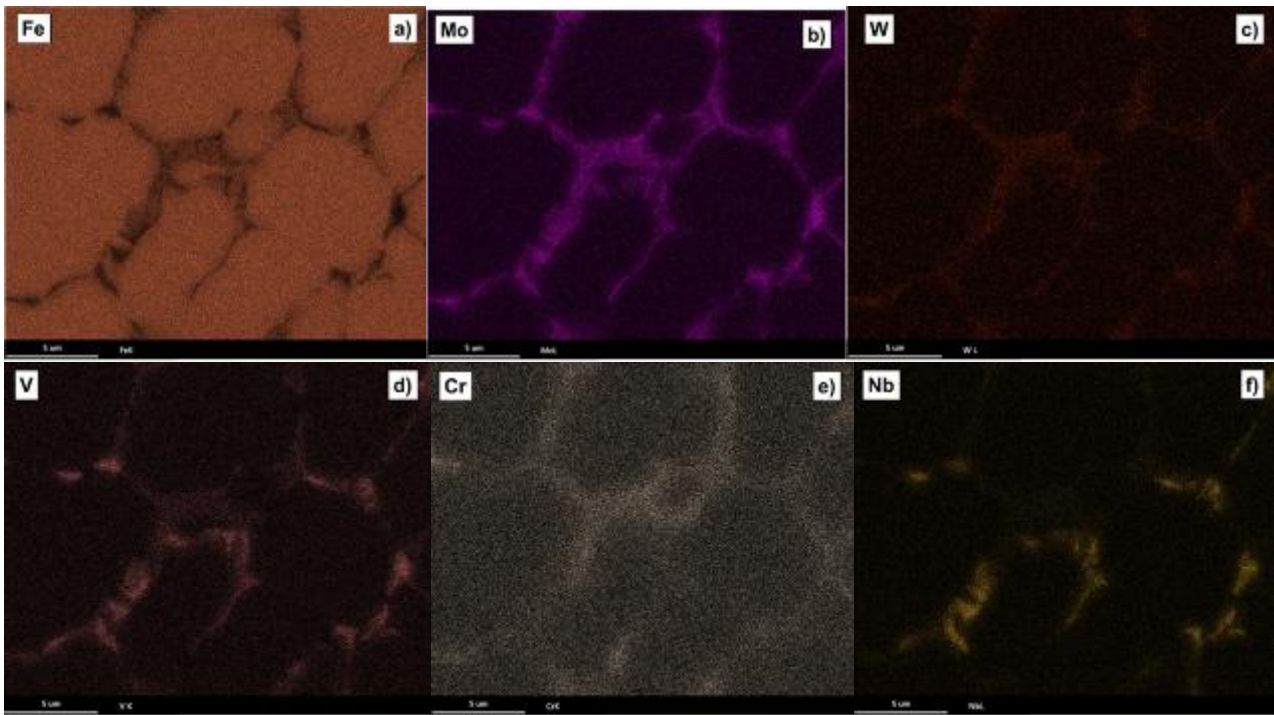


**Figure 3:** EDX mapping of the HSS laser hardfacings with 1 wt.% Nb.

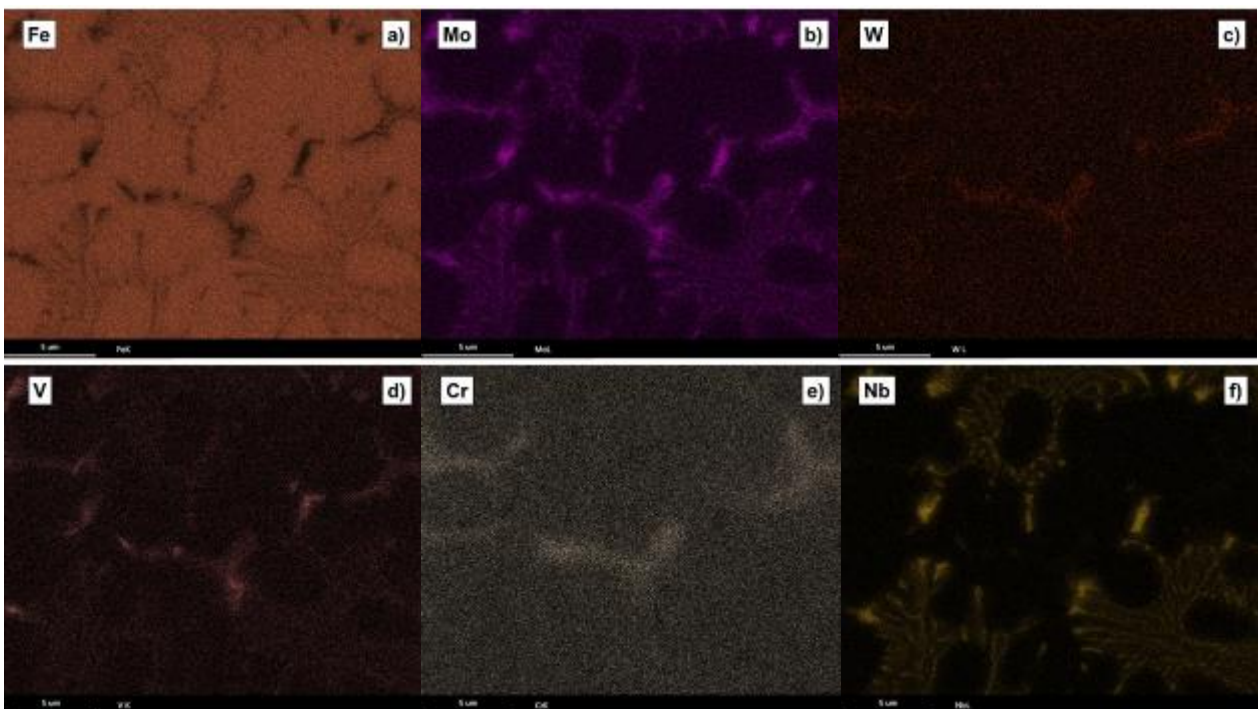


**Figure 4:** EDX mapping of the HSS laser hardfacings with 3 wt.% Nb.

The diagrams of the X-ray diffraction analyses (XRD) are shown in Figure 3. The diagrams show the relevant  $2\theta$ -region for all four niobium concentrations. The reflection positions of the different phases are indicated in the legend. The phase analysis of the reference sample reveals a composition characterized by an  $\alpha$ -iron matrix containing small amounts ( $< 2$  wt.%) of  $\gamma$ -iron due to the presence of retained austenite. Iron carbides are present mainly as  $\text{Fe}_2\text{C}$ , even  $\text{Fe}_7\text{C}_3$  could be measured in smaller amounts (Fig. 3).

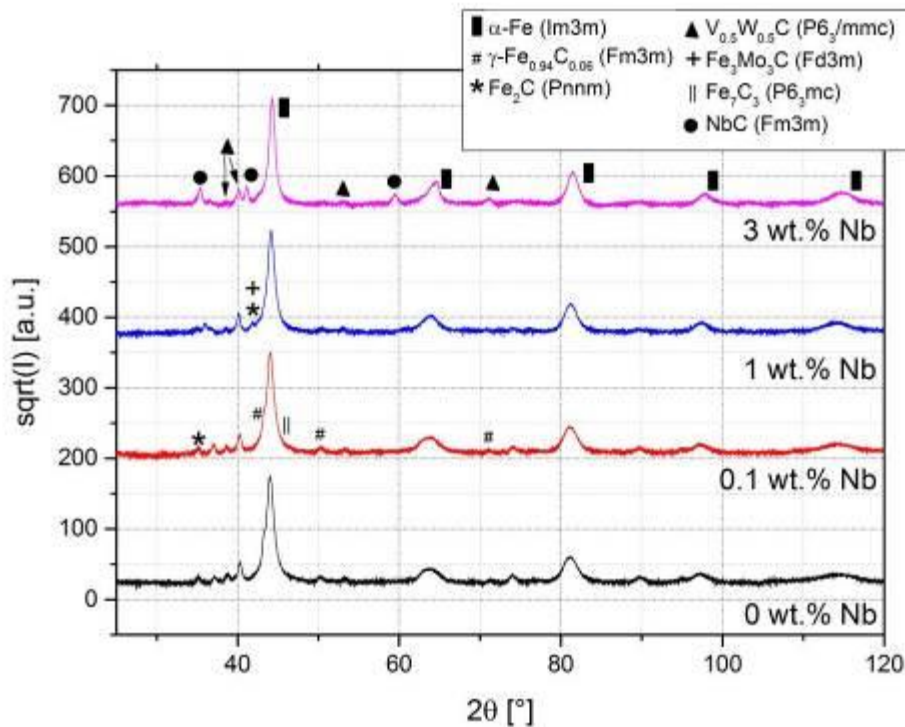


**Figure 3:** X-ray diffraction diagram of the HSS laser hardfacings

Ternary carbides of the present alloying elements (W, Mo, Cr, V) could be measured with the following stoichiometry:  $\text{Fe}_3\text{Mo}_3\text{C}$ ,  $\text{V}_{0.5}\text{W}_{0.5}\text{C}_{0.5}$  and  $\text{Cr}_{0.3}\text{W}_{0.7}\text{C}_{0.5}$ . A similar composition was found for the samples doped with 0.1 and 1% Nb. The presence of carbides containing niobium, namely NbC, was only measurable for the sample with 3% niobium. A quantitative summary of the measurements is given in table 2. The sample containing 0.1 wt.% Nb is not included since according to the diagrams, its composition is very similar to the reference sample. The values are the results of Rietveld refinements of crystallographic phases matched with the PDF data base [20]. The error for the wt.% values are in the range of 1-2%. The results evidence an increase in the amount of Fe(C) and a significant reduction of  $\text{Fe}_2\text{C}$  for increasing Nb contents. The amount of  $\text{M}_2\text{C}$  first increases for Nb concentrations up to 1 wt.% and then slightly decreases for a 3 wt.% Nb content in coincidence with a sudden rise of NbC.

**Table 2.** Crystallographic phase composition for the various Nb doped HSS laser hardfacings.

Crystallo- graphic Phases	Fe(C) Im3m/ Fm3m	V0.5W0.5C0.5/ Cr0.3W0.7C0.5 P63/mmc	Fe2C Pnmm	M3Mo3C Fd3m	M7C3 P63/mmc	NbC Fm3m
Reference	81.1 %	2.2 %	13.7 %	< 2 %	-	-
1 wt.% Nb	88.6 %	3.7 %	4.1 %	< 2 %	< 2 %	-
3 wt.% Nb	87.9 %	2.8 %	-	< 2 %	-	8.3 %

### 3.2 Role of niobium on dendrite arm spacing and carbide content

The dendrite arm spacing was measured using the linear intercept method on SEM images taken at a magnification of 1000x using five lines per hardfacing. The average linear intercept obtained by dividing the line length by the number intercepted dendrite arms was multiplied by 1.57 in order to obtain the average dendrite arm spacing, as recommended by ASTM E112-12. The results highlight the microstructure refinement caused by an increasing Nb content (Table 3). Besides its high affinity for carbon, niobium is well-known for providing sites for nucleation, so that higher Nb contents provide more nuclei during the solidification process, leading to a more refined microstructure.

The quantitative evaluation of the microstructure was performed using the image analysis software Leica QWin. One SEM image of each hardfacing taken with a magnification 1000x was used for performing the phase analyses (Fig.3 a-c). No repetitions were performed since the number of dendrites present in the micrograph was large enough to be statistically representative. The pixels of the image were assigned to a given phase according to the following criteria: grey level pixels were attributed to the iron matrix, white pixels to carbides and black pixels to porosity of the hardfacing. The image quantification of the microstructure was limited to samples with up to 1 wt.% Nb, since their microstructural composition features a very clear distinction between martensitic matrix and carbide networks. The samples containing 3 wt.% Nb were not considered for these analyses, since their more complex carbide structure is not suitable for image analysis.

The results show that when increasing the niobium content up to 1 wt.%, the surface covered by the carbide networks along the grain boundaries diminishes from 16 to 11 %. As a consequence, the area covered by the martensitic dendrites rises from 83 % for the reference hardfacing to a value of almost 89 % for a Nb content of 1 wt.%. In all cases, the observed porosity of the samples was below 0.5 %.

**Table 3:** Dendrite arm spacing, surface coverage in % of the matrix (dark grey in SEM images, Fig. 3) and carbides (light grey in SEM images, Fig. 3) as a function of niobium content

Hardfacing	Dendrite arm spacing ( $\mu\text{m}$ )	Surface coverage of dendrites (%)	Surface coverage of carbides (%)	Porosity (%)
Reference	$18.8 \pm 2.7$	83.0	16.5	< 0.5
0.1 wt.% Nb	$12.0 \pm 1.7$	83.4	16.6	< 0.1
1 wt.% Nb	$11.8 \pm 1.6$	88.6	11.3	< 0.1
3 wt.% Nb	$10.7 \pm 0.5$	-	-	-

### 3.3 Hardness of the hardfacings and nano-hardness of the martensitic dendrites

Macroscopic hardness of the samples was measured in the cross-section of the hardfacings using Vickers HV30. The hardness measurements had a very high reproducibility. The hardness of the reference hardfacing had a value of  $776 \pm 10$  HV30 and the hardness of the hardfacings with 0.1 and 1 wt.% niobium content lay within the standard deviation of the reference sample, with values of  $769 \pm 7$  and  $778 \pm 9$  HV30, respectively. Hence, the results show that niobium content does not modify the macroscopic hardness of the hardfacings for amounts equal or smaller than 1 wt.% (Table 4). For a larger Nb content of 3 wt.%, hardness decreases by over 20 % down to a value of  $612 \pm 20$  HV30.

**Table 4:** Macroscopic Vickers Hardness HV30 as a function of niobium content.

Hardfacing	Vickers Hardness (HV30)
Reference	$776 \pm 10$
0.1 wt.% Nb	$769 \pm 7$
1 wt.% Nb	$778 \pm 9$
3 wt.% Nb	$612 \pm 20$

The morphology of the Vickers indents was inspected in a light microscope after etching the cross-sections (Fig. 4). The analyses showed that indentations performed on hardfacings with up to 1 wt.% Nb content mostly had one or two radial cracks initiating at the corners of the Vickers imprints or on their vicinity. Under SEM it can be observed that the cracks tend to run along the intergranular carbide network, as long as it is favourably oriented to the direction of crack propagation. Otherwise, the cracks switch from intergranular to transgranular propagation through the martensitic dendrites until a favourable carbide network is found. No cracks could be observed for the samples containing 3 wt.% Nb indicating a higher fracture toughness for these hardfacings.

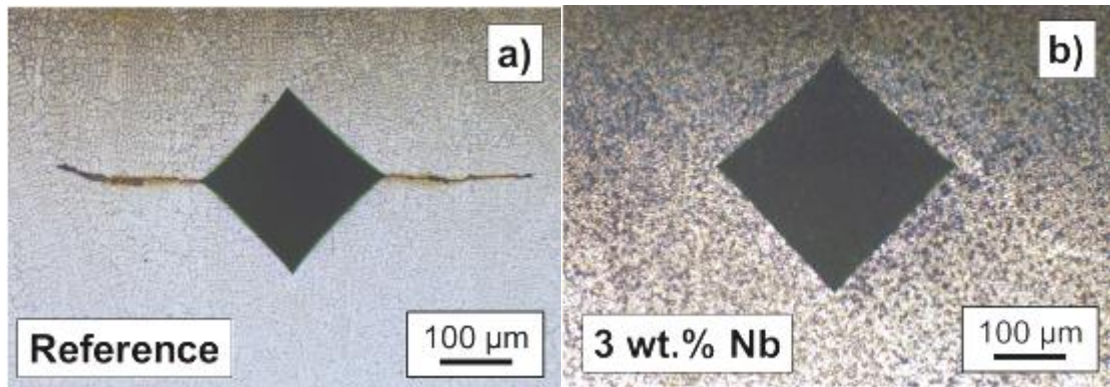


**Figure 4:** Macroscopic Vickers Hardness HV30 imprints on a reference HSS laser hardfacing (a) and a hardfacing doped with 3 wt.% Nb (b).

Despite the differences observed at the microstructural level, the macroscopic hardness of the hardfacings remained unaffected by niobium contents of up to 1%. For this reason, instrumented nanoindentation measurements were performed in order to reveal any potential impact of the different chemical composition and microstructure on the mechanical properties of the hardfacings. The nanoindents were performed on the cross-sections of samples containing 0 and 1 wt.% Nb. In order to identify the carbide networks and verify that all nanoindents were performed inside the martensitic dendrites, the nanoindenter was used in scanning probe microscopy imaging mode. The results of the instrumented nanoindentations were evaluated in terms of hardness  $H$  and reduced Young's Modulus  $E_r$ , with  $1/E_r = (1-\nu_d^2)/E_d + (1-\nu_s^2)/E_s$ ,  $\nu$  being the Poisson ratio and the subindex  $d$  and  $s$  denoting the diamond indenter tip and the sample hardfacing, respectively.

The matrix nanohardness of the reference hardfacing has a value of  $12.0 \pm 0.5$  GPa. A slightly lower hardness could be measure for the sample containing 1 wt.% Nb, namely  $11.8 \pm 0.3$  (Fig. 6a). However, the difference is not statistically representative, since the standard deviation of both measurements clearly overlap each other, despite the very low scattering of the measurements (standard deviation lower than 5%). On the other hand, the reduced Young's Modulus of the sample containing 1 wt.% Nb was measured to be about 10 % lower compared to the reference sample. The values measured were 225 and 208 GPa for the reference and 1 wt.% sample, respectively (Table 5). In this case, the average values of the ten indents are clearly outside their respective error bars.

These results show that the hardness of the hardfacings is not affected by niobium contents up to 1 wt.% either at the macroscopic or at the microscopic level. However, a significant change in the reduced Young's Modulus of the matrix could be measured. This means that although the hardness of the hardfacings remains unaffected for small niobium contents (<1 wt.%), there is a change in the elastic strain to failure, defined as  $H/E_r$ . A higher elastic strain to failure, in this case lower  $E_r$ , is associated with a higher resistance to cracking in coatings and a higher resistance to wear and failure. Furthermore, a lower value of  $E_r$  is desirable since for a given load, the contact pressure will be distributed over a larger contact area, which increases the elastic strain to failure and the resistance of the coating to cracking [27].

**Table 5:** Instrumented nanoindentation measurements of the martensitic dendrites for the reference HSS laser hardfacing and the hardfacing doped with 1 wt.% Nb.

Hardfacing	Hardness (GPa)	Reduced Young's Modulus (GPa)
Reference	12.0 ± 0.5	225 ± 4
1 wt.% Nb	11.8 ± 0.3	208 ± 3

### 3.4 Abrasion resistance

The abrasion resistance of the high speed steel hardfacings was evaluated using a rubber wheel test. Under this testing procedure, the samples undergo low stress contact conditions. The results show that the reference sample has the poorest abrasion resistance (Fig. 5). Microalloying the hardfacing with 0.1 wt.% Nb results in an improvement of the abrasion resistance of about 8%. The best performance is observed for the hardfacing containing 1 wt.% Nb, which shows an improvement of the wear rate over a factor two better than the reference sample. For the hardfacing with the highest amount of Nb (3 wt.%), the wear rate rises slightly compared to the best performer, but only up to a value about half the wear rate of the reference sample.

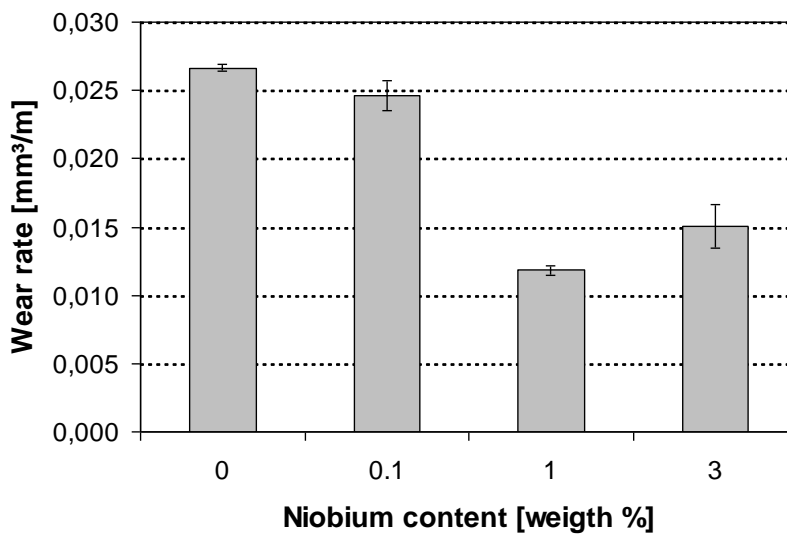


**Figure 5:** Wear rate for HSS laser hardfacings tested under low-stress abrasion conditions as a function of the niobium content

An initial optical inspection of the tested samples indicates significant differences in the surface appearance. For this reason, the wear scars were investigated using 3D microscopy. The results show relevant differences in the wear scars in terms of surface topography. Hardfacings with a niobium content up to 1 wt.% show shiny wear scars characterised by the presence of abrasion marks (Fig. 6a). In contrast, hardfacings with 3 wt.% Nb present a rough and wavy surface with fewer abrasion marks, which suggests a higher degree of plastic deformation and hence a higher ductility (Fig. 6b).

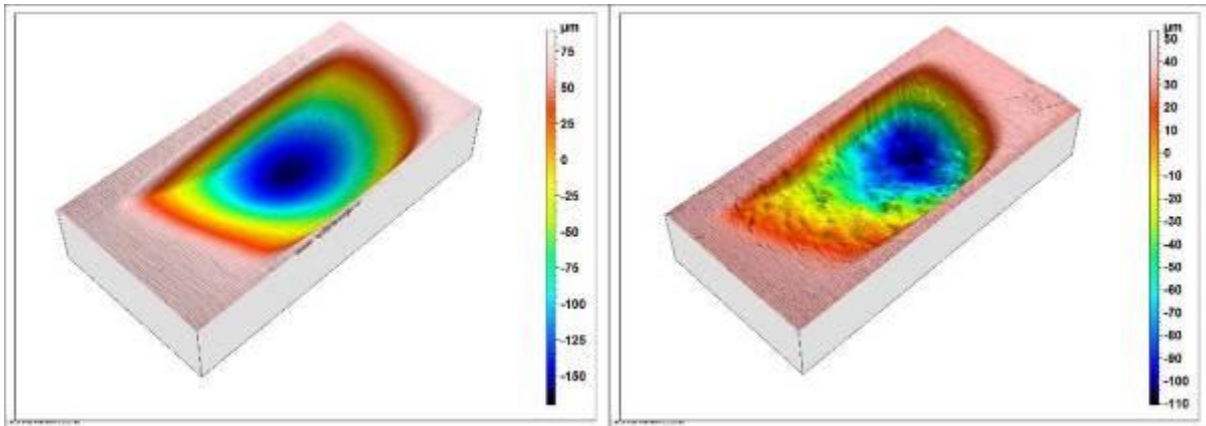


**Figure 6:** Surface topography of HSS laser hardfacings tested under abrasion. Reference sample (a), sample with 3 wt.% Nb (b). Note the different scale in both figures due to the large difference in wear scar depth.

Further insights into the dominant wear mechanisms were obtained by analysing the tested surfaces using SEM. Surface analyses of tested surfaces show the presence of abrasion grooves, which indicate material removal by wedge formation and microcutting (Fig. 7). For samples with niobium contents of up to 1 wt.%, cracks running in parallel are sporadically observed in some of the deeper abrasion marks (Fig. 7b and 7c). These cracks appear to follow a more ductile mechanism in samples with 1 wt.% Nb content (Fig. 7c). In general, the width of the abrasion marks increases for higher niobium contents (Fig. 7d). Intergranular carbides become more visible under secondary electrons for higher Nb contents, indicating that the carbides are protruding out of the surface due to wash out of the iron matrix. As a consequence, a rise in the niobium content of a sample is accompanied by an increasing amount of carbide pull out. Carbide pull out is seldom observed in the reference sample, whereas it increases dramatically for contents of 1 wt.% Nb and higher.

An example comprising all these wear mechanisms can be observed on the sample with 3 % Nb content. Its surface is characterised by the presence of deep microcutting marks, salient intergranular carbides, severe carbide pull out and abrasive embedment (Fig. 7d). Further, this sample is the one that contains the highest number of deep ploughings running not parallel to the sliding direction. Abrasive embedment in the martensitic matrix is observed sporadically for samples containing up to 1 wt.% Nb and in a much larger extent in samples with 3 wt.%. Longitudinal cross-sections of the tested hardfacings show no signs of near-surface microstructural damage. Neither plastic deformation nor cracks could be observed in the sub-surface region of the hardfacings for any Nb concentration.

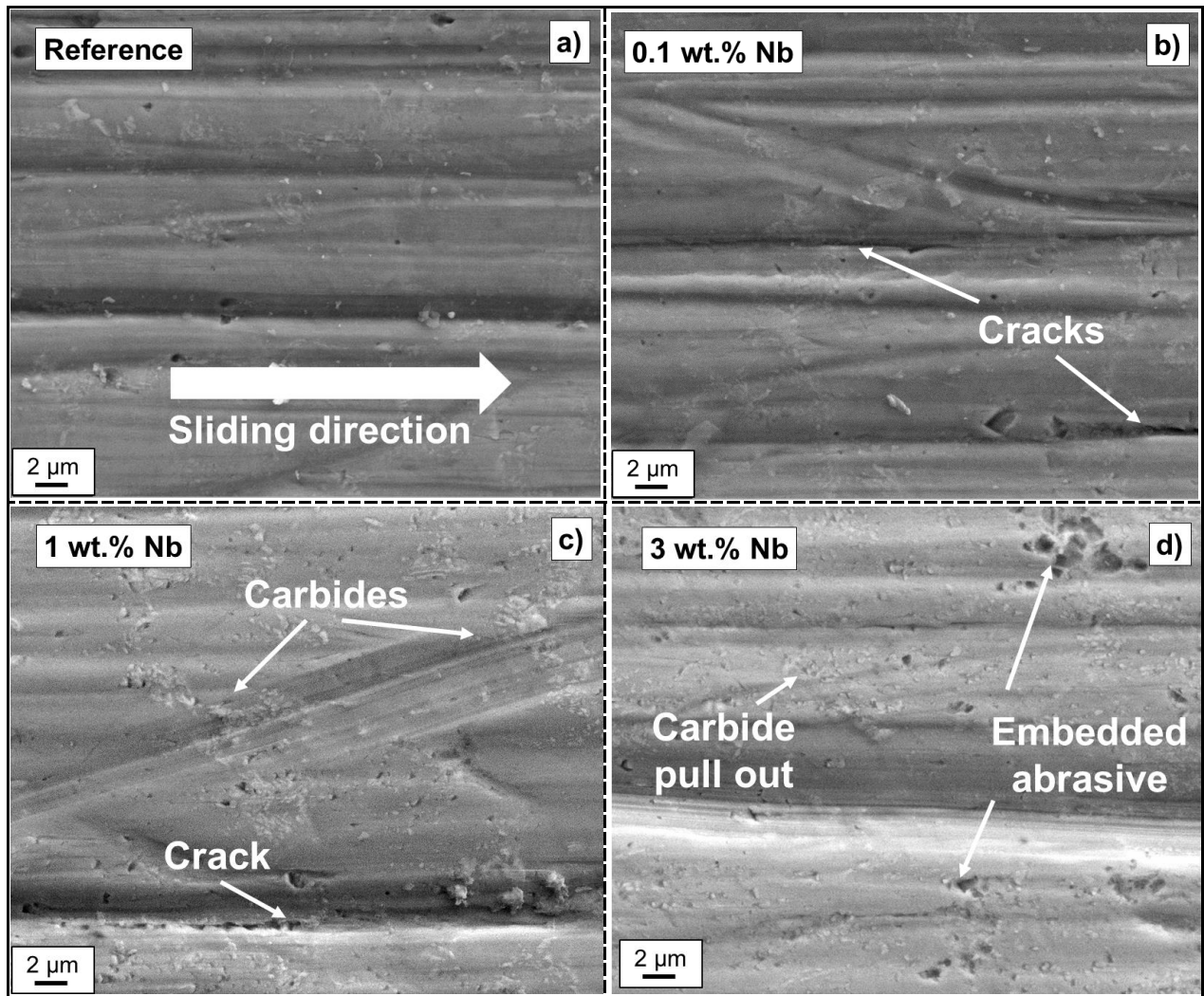


**Figure 7:** SEM micrographs of HSS laser hardfacings surfaces tested under abrasion. Reference hardfacing (a), 0.1 (b), 1 (c) and 3 wt.% Nb (d). The sliding direction is the same for all samples and is shown in (a).

### 3.5 Erosion resistance

The resistance of the high speed steel hardfacings to erosion under high stress conditions was investigated using a high speed slurry erosion tester. During the test, the abrasive is crashed against the sample under high stress conditions, causing the initial abrasive size of 8-10 mm to be reduced down to 0-2 mm in average size. The cumulative mass loss of the tested samples was gravimetrically measured and it is plot as a function of the hardfacings Nb content (Fig. 8). The results show a mass loss of 1.8 g for the reference sample. A decrease in mass loss of 8 % is observed for the hardfacing containing 0.1 wt.% niobium. For higher niobium contents, the mass loss during the tests tends to increase again. Samples with 1 wt.% Nb content had a similar performance as the reference samples, whereas samples with 3 wt.% Nb had even a slightly worse performance when compared to the reference material. The results also show that hardfacings with



a niobium content of 0.1 wt.% provided the highest reproducibility, having hence the lowest standard deviation.

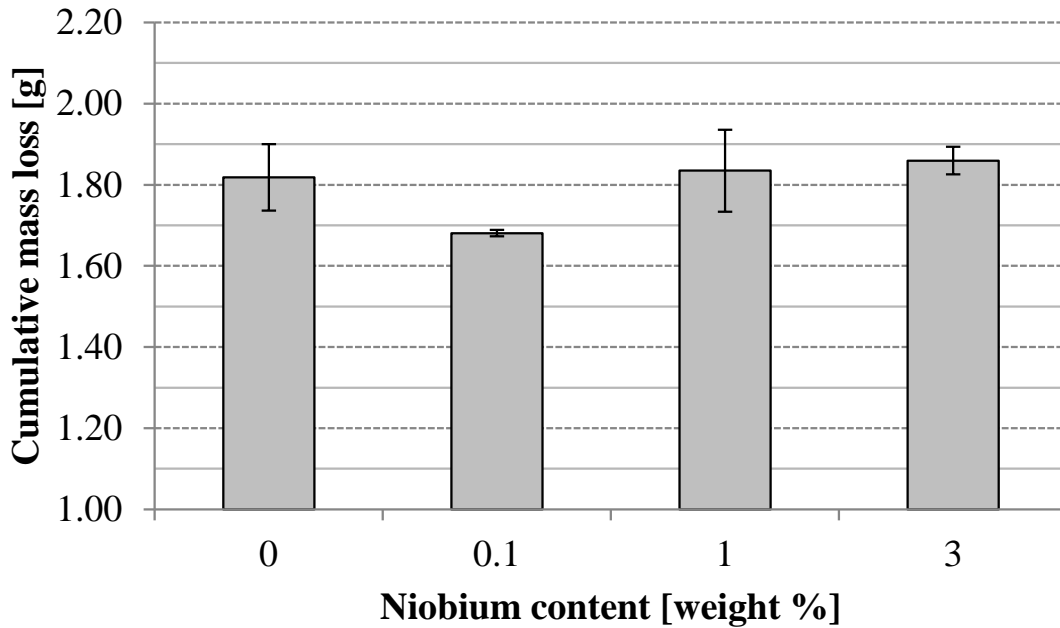


**Figure 8:** Cumulative mass loss during the slurry erosion tests as a function of niobium content

The surface of tested samples was analysed using scanning electron microscopy. The investigations were focused on evaluating the edge resistance of the hardfacing upon impact with the abrasive particles. Due to the fluid flow patterns within the slurry pot, the damage induced to the samples is slightly asymmetric, being the material loss higher in the lower corner of the tested samples [22]. Consequently, SEM micrographs were taken at the lower and upper edge of the hardfacings. In general, the topography of the tested surfaces is characterised by the presence of microcutting and indentation marks created by the impact with the abrasive, thus leading to abrasive erosion [28].

Remains of fractured abrasive with typical size of about 10 to 20  $\mu\text{m}$  are found embedded throughout the surface of the samples when using backscattered electrons. The amount and size of embedded abrasive particles increases for higher Nb contents at the lower edge of the hardfacings, in particular for 3 wt.% Nb content, indicating a higher ductility. Carbide pull out is present in all samples, but the occurrence is significantly higher for samples with a higher amount of niobium. In general, deeper grooves and indentation impacts are observed for higher niobium contents.

The upper corner surface of the reference sample shows a topography dominated by the presence of mild cutting marks with sporadic presence of impacts. The surface is rather smooth and the grooves are mostly aligned in the same direction. For 0.1 and 1 wt.% Nb, the topography is dominated by impact marks and the microcutting marks are significantly scarcer and shorter compared to the reference. No preferred direction is observed. In contrast, the 3 wt.% Nb hardfacing shows mostly

aligned ploughing marks, which are deeper when compared to the reference sample. In the lower corner, all hardfacings have a topography dominated by the presence of impact marks with fewer and shorter grooves (Fig. 9). The severity of the impacts increases for higher Nb contents. The reference sample presents a rather smooth surface with shallow indents and short microcuts. Deeper indents and microcuts can be observed in samples with a Nb content of 0.1 wt.%. When increasing the Nb content to 1 wt.%, microcuts are even deeper and often the presence of partly formed chips can be seen. The sample doped with 3 wt.% Nb presents a very rough surface due to the large amount of impact indents and wedges formed by the abrasive particles upon impact.

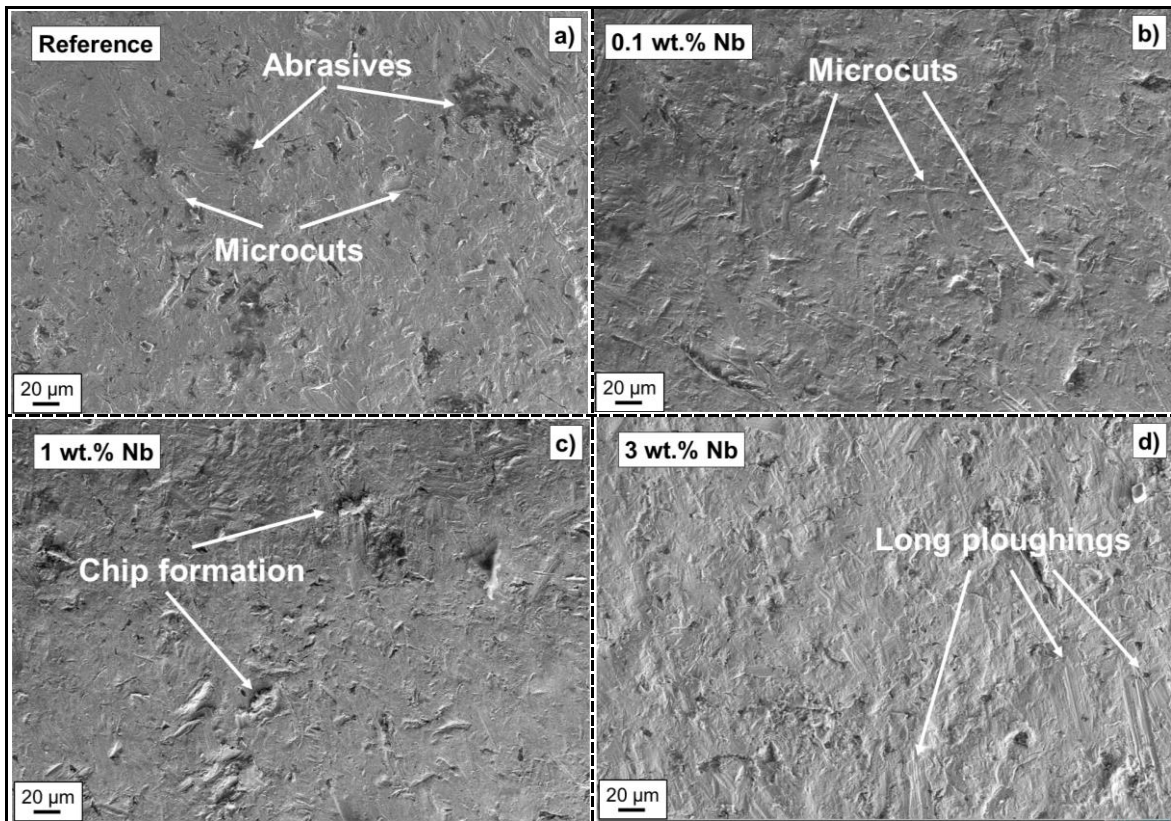


**Figure 9:** SEM micrographs of HSS laser hardfacings tested under slurry erosion

These observations are confirmed when analysing the cross-sections of the investigated samples (Fig. 10). The reference sample has a rather straight surface, which indicates a more brittle material removal mechanism. Sporadically, some plastically deformed indent imprints can be observed. Their dimensions are typically small and are produced always in the more ductile martensitic dendrites, where there is no presence of carbides. The hardfacings with 0.1 and 1 wt.% Nb content presents a similar cross-section, even though the amount and severity of the indents increases with increasing Nb content. Finally, the hardfacing with 3 wt.% Nb content shows a rougher surface but with shallower indents. Sporadically, carbide cracks are observed at a depth of about 20 to 30 μm. In general, the results show the trend that for higher Nb contents the ductility of the hardfacing steadily increases.

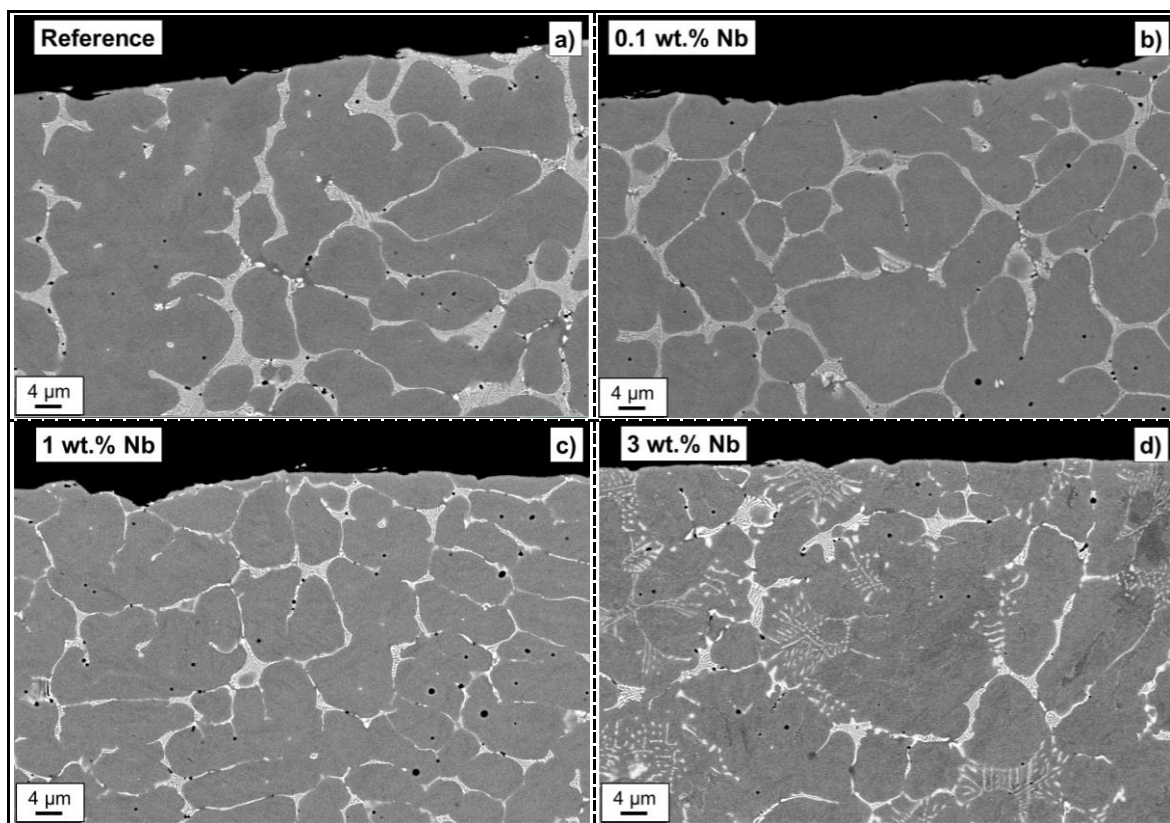


**Figure 10:** SEM micrographs of HSS laser hardfacing cross-section tested under slurry erosion.

### 3.6 Corrosion resistance

The corrosion behaviour of the hardfacings was evaluated using potentiodynamic polarization scans in acidic media. In general, high speed steel hardfacings with low Cr content are developed for providing superb wear resistance in high demanding applications, such as cutting, but are not meant to offer corrosion protection. However, in many cutting applications, such as the woodworking or food industry, high speed steels are expected to perform satisfactorily under acidic media [29]. The influence of changing the anion on the corrosion behavior of powder metallurgical M2 high speed steel was addressed by Brett et al. using several voltammetry techniques [30]. They found that out of six investigated anions, sulfates were the most aggressive towards HSS.

Hence the corrosion behaviour of niobium containing hardfacings was evaluated in 0.5 M H<sub>2</sub>SO<sub>4</sub> solution and the results obtained are shown in Fig. 11. Regardless of the hardfacing tested, the primary passivation potential was approximately +0.2 V and no obvious shift could be observed under these conditions for increasing Nb concentrations. However, the effect of Nb alloying on the onset of the passive region can be clearly distinguished. These regions were between +1.0 V and +1.2 V versus Ag/AgCl for the reference, 0.1 and 1 wt.% Nb-doped hardfacings. On the other hand, the earlier onset of the passive region (+0.8 V versus Ag/AgCl) for the 3 wt.% Nb-doped HSS reflects the greater ability of this material to passivate. The appearance of two peaks in the anodic region of the polarization curves for the reference hardfacing and hardfacings doped with lower amounts of Nb (0.1 and 1 wt.%) is probably related to electrochemical reactions in the solid state

involving the transition to higher oxidation states of Cr, Mo and W, as previously reported in literature [31–33]. These peaks become much more attenuated in case of the 3 wt.% Nb hardfacing, suggesting a possible inhibition of these electrochemical reactions.

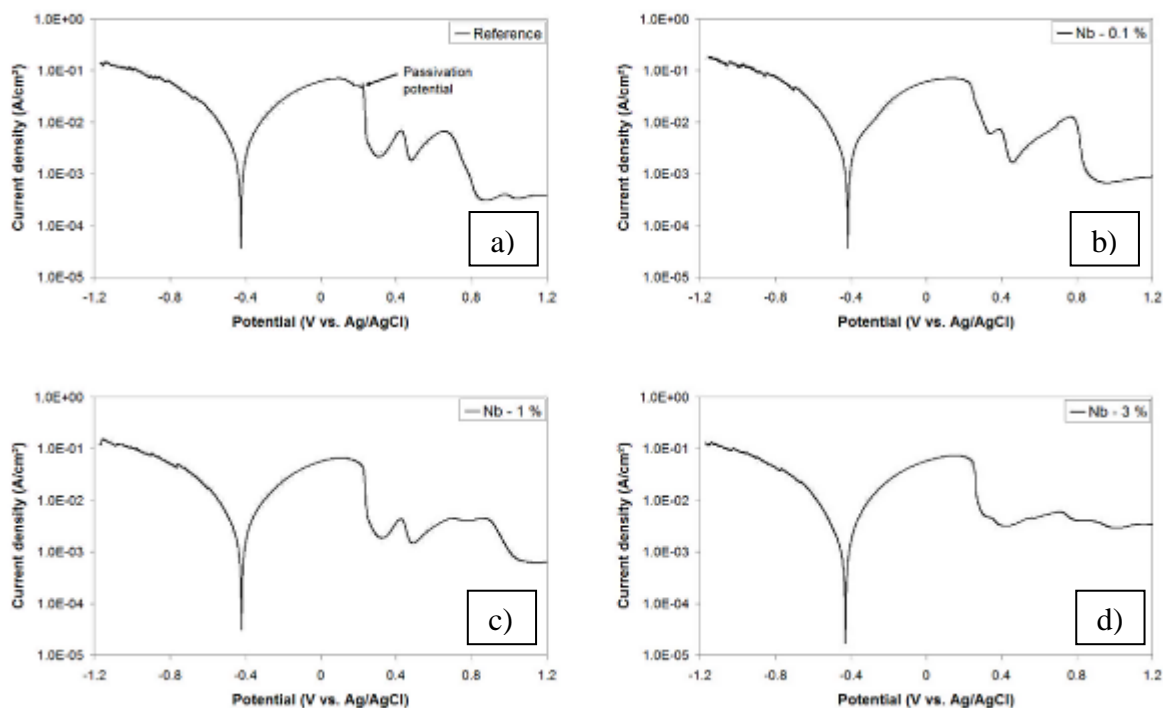


**Figure 11:** Potentiodynamic polarization curves of the HSS laser hardfacings in 0.5 M H<sub>2</sub>SO<sub>4</sub> solution

After the potentiodynamic polarization curves, the corrosion scales formed on the surface of the high speed steel hardfacings was analysed using SEM. The corrosion layer formed on the reference hardfacing is discontinuous and has a “mud-cracked” structure (Fig. 12 a). The layer is not very dense and has a high porosity (Fig. 12 b). With increasing Nb content the scale layer becomes more continuous and the parts of the surface not covered by the corrosion products became scarcer (Fig. 12 c). Additionally, the layer becomes denser (Fig. 12 d). The EDX analyses showed that the corrosion layer is mainly formed by iron oxides, with the presence of alloying elements and carbon. Nb was detected for hardfacings with a content higher than 1 wt.%.

Since Nb has a higher affinity towards carbon, when compared to Cr, an increase of Nb content means that less C is available to form chromium carbides, so that Cr remains in elemental form dissolved in the matrix, thus boosting the corrosion resistance of the hardfacing. The denser corrosion layer observed for the hardfacing with 3 wt.% Nb content is believed to be responsible for suppressing the peaks observed in the anodic domain. Despite this improvement, even a 3 wt.% of Nb content is not enough for providing a complete surface passivation.

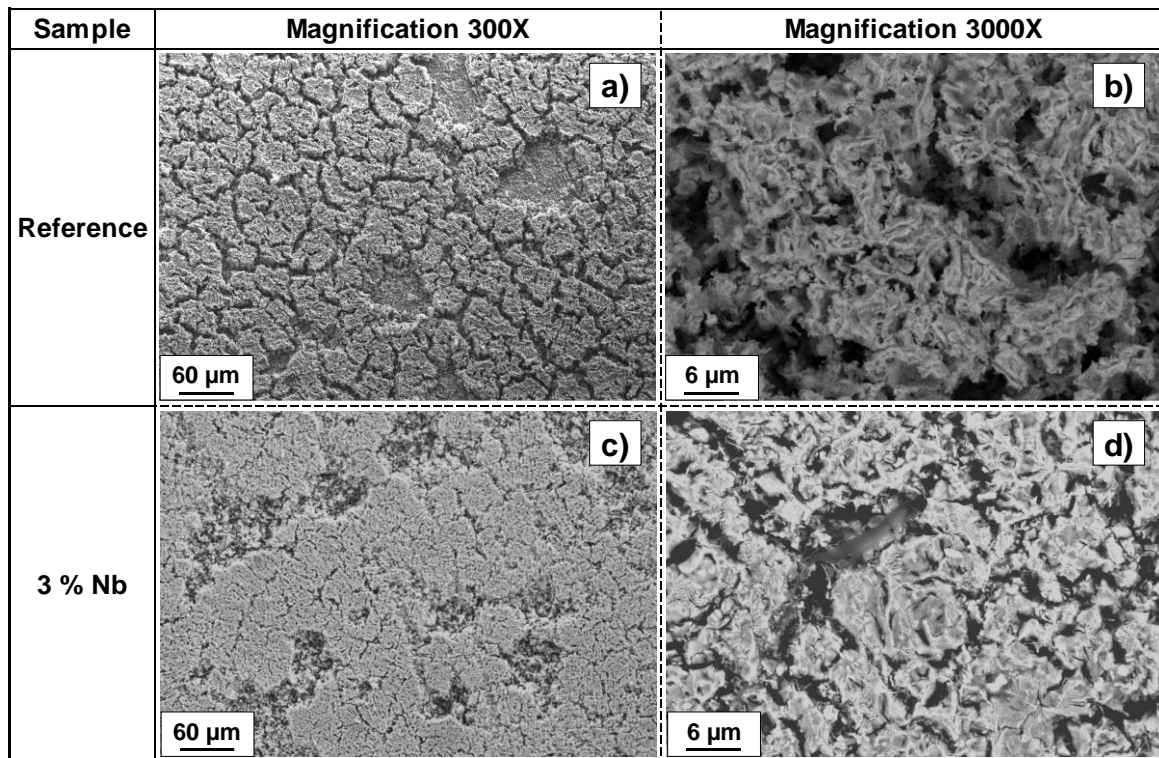


**Figure 12:** SEM analyses of the corrosion layer present on the HSS laser hardfacings after potentiodynamic tests.

## 4. Discussion

The present work shows the impact of niobium content on the microstructure of high speed steel hardfacings and their resulting mechanical and chemical properties. Under the absence of niobium, the hardfacings have a well-known microstructure characterised by the presence of fine  $M_6C$  and  $M_2C$  carbide networks surrounding the martensitic dendrites. This microstructure is responsible for providing HSS hardfacings with high hardness and excellent wear resistance. However, the toughness of laser hardfacings is sometimes not adequate due to the high cooling rates undergone during the deposition process, which result in a high cracking susceptibility and an excess of brittleness in operation [7,8]. In order to enhance toughness of laser hardfacings, two main parameters can be modified: heat treatment of the hardfacing during or after deposition or chemical composition of the alloy. A modification of the chemical composition is often preferred for economic reasons. In contrast to bulk materials used for tools, hardfacings are mostly used in an as-deposited condition. Hence, the presented approach of doping HSS with niobium pursues this goal.

A first impact of niobium on the microstructure of HSS hardfacings is on **dendrite arm spacing** refinement. It was observed that alloying with niobium even for concentrations up to 1% is sufficient to reduce dendrite arm spacing up to 36 %, while maintaining hardness of the undoped hardfacing. **In our case, the microstructural refinement does not reach the order of magnitude achieved by Hemmati et al. in Ni-based alloys due to the different solidification behaviour [8]. In**

any case, a smaller average grain size is known to be beneficial. Smaller grains sizes provide higher hardness by the Hall-Petch effect, while improving plasticity [8]. Dendrite arm spacing can be further reduced for larger niobium concentrations but at the expense of altering the microstructure with additional intragranular niobium-rich carbide structures. In this case, hardness at the macroscopic level becomes hampered.

Besides a finer dendrite arm spacing, niobium-doped hardfacings also have intergranular carbides with a smaller width. These carbides in HSS laser hardfacings are typically molybdenum and tungsten rich  $M_6C$  and  $M_2C$  carbides. When having niobium as doping element, the amount of available carbon for Mo, W, Cr and V carbide formation is reduced, due to the higher affinity of niobium for carbon. As shown, the amount of Nb found solved in the matrix was negligible for all HSS laser hardfacings independently of the Nb content. In contrast, as a result of the lower carbon availability, part of the other carbide forming elements have to remain solved in the matrix. Since niobium tends to form preferentially monocarbides, a higher amount of Nb rich MC results in a higher amount of dissolved Mo and W in the matrix, since these elements are mostly  $M_6C$  and  $M_2C$  carbide formers in this system. Due to the stoichiometry, the total amount of carbides is reduced. Carbides are essential for providing a superior hardness and wear resistance. However, due to their brittleness, they are also a source for crack initiation and propagation, hampering the overall toughness of the material. The loss of macroscopic hardness in Nb-doped laser hardfacings due to the lower amount of carbides seems to be compensated in the present case by the higher hardness of MC carbides (~2800 HV) when compared to  $M_2C$  (~2200 HV) but especially in comparison to  $M_6C$  (~1650 HV) [34].

A third factor contributing to the improvement of the toughness of the HSS laser hardfacings was found by nanoindentation. The nanohardness of the martensitic dendrites does not change significantly when comparing the reference HSS hardfacings with hardfacings doped with 1 wt.% Nb. However, the elastic modulus of the dendrites is lower, which benefits the elastic strain to failure of the hardfacing ( $H/E_r$  ratio) and, consequently, boosts its resistance to cracking. The combination of smaller dendrite arm spacing with a lower amount of intergranular carbides accompanied by a higher elastic strain to failure of the matrix contributes to maintain macroscopic hardness while improving toughness. As a result, the abrasion and erosion resistance of the laser hardfacings is improved. Abrasive wear resistance of laser hardfacings can usually be well correlated to material hardness and carbide content at room temperature conditions. Erosion and impact wear resistance is usually correlated with a tough matrix with fine disperse carbides [2,5].

In our case, a higher Nb content is beneficial for improving abrasive wear resistance. Up to Nb concentrations of 1 wt.%, abrasion resistance improves by over a factor two, despite all hardfacings having the same macroscopic hardness. These results can be explained in terms of the higher matrix ductility. As revealed by SEM micrographs, a higher Nb concentration leads to microcutting combined with matrix deformation by ploughing and carbide pull out. As a result, part of the

abrasive damage is accommodated by plastic deformation, which results in lower wear. The larger amount of dissolved carbide forming elements in the matrix for higher Nb contents may also contribute by solid solution strengthening. In case of 3 wt.% Nb content, the lower hardness with seemingly increased ductility results in a very good abrasion resistance, despite being the softer hardfacing. In this case, the hard intergranular niobium rich MC carbides along with a finer microstructure, i.e. a smaller interparticle distance, may compensate for the hardness drop.

In the slurry erosion tests, impact resistance and edge stability play a crucial role. Under these conditions, the undoped HSS laser hardfacing was shown to wear by a rather brittle mechanism. The surfaces had a smooth topography with lack of indents, despite the vast amount of material removed. Addition of Nb results in a progressive switch towards a more ductile mechanism. This is confirmed by the presence of partly removed chips for the 1 wt.% Nb hardfacing. For 3 wt.% Nb, the ductility is remarkable, which is highlighted by the shallower indents and rougher surface in the sample cross-section. Combined with the surface micrograph, this confirms that the sample is so ductile that most of the material becomes easily removed by microcutting. In consequence, it can be ascertained that the failure mechanism changes substantially with increasing niobium content, despite the overall wear rate of the HSS laser hardfacings being similar. In this case, microalloying with 0.1 wt.% Nb was shown to be a good balance between toughness and erosion resistance.

A positive side effect of the high carbon affinity of niobium is that a major amount of chromium remains solved in the matrix to provide added corrosion protection. Obviously, due to their small chromium content, HSS laser hardfacings are not passive materials. Nevertheless, the better corrosion resistance observed for increasing Nb contents is expected to boost the performance of these hardfacings under cutting application in food and wood industry due to a better resistance against acidic corrosion. The mud-cracked structured surfaces of laser HSS hardfacings observed after the potentiodynamic tests is in agreement with the results obtained by Alves et al [35] for bulk M2 HSS with a very similar composition and having mostly  $M_6C$ ,  $M_{23}C_6$  and  $M_4C_3$  carbides. In their case, they compared the corrosion resistance before and after heat treatment of the HSS and found that before heat treatment HSS has a superior corrosion performance. The reason is secondary precipitation of carbides solved in the matrix after the thermal treatment, in particular chromium, which hampers the corrosion properties of the material.

To sum up, it can be concluded that doping with niobium is beneficial for improving the toughness of HSS laser hardfacings, while maintaining their strength. The optimum doping amount depends on the application. Microalloying (0.1 wt.% Nb) is beneficial for improving the erosion and high stress abrasion resistance for applications such as mining. For low stress abrasion applications, such as agriculture, a higher niobium content of 1 wt.% is favourable. A balance between better toughness, corrosion protection and good abrasion performance can be reached for 3 wt.% Nb. This amount of doping could be promising for applications such as cutting in wood and food industry, where a certain amount of corrosion resistance against acidic media is expected.

## 5. Conclusions

High speed steel hardfacings with different niobium contents were deposited using a high-power direct diode laser. The influence of niobium content on the hardfacing microstructure and the resulting mechanical properties were characterised using microscopy, macro and nanoindentation. Niobium content has an impact on the hardfacings by reducing their **dendrite arm spacing**, reducing carbide content and increasing elastic strain to failure. These microstructural changes result in an improvement of the hardfacing toughness, while maintaining the hardness for Nb contents up to 1 wt.%. These enhanced mechanical and chemical properties result in an improvement of low stress abrasive wear and corrosion resistance. The erosion resistance is less influenced by the niobium content. Here, a clear benefit can only be achieved by microalloying (0.1 wt.% Nb), which proved to be a good compromise between ductility and erosion resistance.

## 6. Acknowledgements

This work was funded by the Austrian COMET-Program (Project K2 XTribology, Grant No. 849109), and has been carried out within the Excellence Centre of Tribology. The work at Tampere University of Technology has been done within the FIMECC BSA (Breakthrough Steels and Applications) programme. We gratefully acknowledge the financial support from the Finnish Funding Agency for Innovation (Tekes) and the participating companies. The authors are indebted to Dr. Christian Jogl and Dr. Jaroslav Wosik for performing the SEM analyses, Ms. Fjorda Xhiku for the 3D microscopy measurements and Mr. Kurt Pichelbauer and Mr. Peter Jandl for depositing the hardfacings.

## 7. References

- [1] N. Yüksel, S. Şahin, *Mater. Des.* 58 (2014) 491–498.
- [2] A. Zikin, I. Hussainova, C. Katsich, E. Badisch, C. Tomastik, *Surf. Coatings Technol.* 206 (2012) 4270–4278.
- [3] J. Hornung, a. Zikin, K. Pichelbauer, M. Kalin, M. Kirchgaßner, *Mater. Sci. Eng. A* 576 (2013) 243–251.
- [4] R. Veinthal, F. Sergejev, A. Zikin, R. Tarbe, J. Hornung, *Wear* 301 (2013) 102–108.
- [5] C. Katsich, E. Badisch, *Surf. Coatings Technol.* 206 (2011) 1062–1068.
- [6] C.-M. Chang, L.-H. Chen, C.-M. Lin, J.-H. Chen, C.-M. Fan, W. Wu, *Surf. Coatings Technol.* 205 (2010) 245–250.



- [7] I. Hemmati, V. Ocelík, J.T.M. De Hosson, *Mater. Sci. Eng. A* 582 (2013) 305–315.
- [8] I. Hemmati, R.M. Huizenga, V. Ocelík, J.T.M. De Hosson, *Acta Mater.* 61 (2013) 6061–6070.
- [9] V. Ocelík, I. Furár, J.T.M. De Hosson, *Acta Mater.* 58 (2010) 6763–6772.
- [10] A. Conde, F. Zubiri, Y.J. de Damborenea, *Mater. Sci. Eng. A* 334 (2002) 233–238.
- [11] F. Weng, C. Chen, H. Yu, *Mater. Des.* 58 (2014) 412–425.
- [12] S. Huth, N. Krasokha, W. Theisen, *Wear* 267 (2009) 449–457.
- [13] W. Theisen, S. Siebert, S. Hurth, *Steel Res. Int.* 78 (2007) 921–928.
- [14] X. Zhi, J. Xing, H. Fu, B. Xiao, *Mater. Lett.* 62 (2008) 857–860.
- [15] M. Filipovic, Z. Kamberovic, M. Korac, M. Gavrilovski, *Mater. Des.* 47 (2013) 41–48.
- [16] L. Zhang, D. Sun, H. Yu, *Mater. Sci. Eng. A* 490 (2008) 57–61.
- [17] F. Scandella, R. Scandella, *Mater. Sci. Technol.* 20 (2004) 93–105.
- [18] H.B. Wang, L.G. Hou, J.X. Zhang, L. Lu, H. Cui, J.F. Huang, J.S. Zhang, *Materwiss. Werksttech.* 45 (2014) 689–698.
- [19] L.A. Dobrzański, A. Zarychta, M. Ligarski, *J. Mater. Process. Technol.* 63 (1997) 531–541.
- [20] T. Degen, M. Sadki, E. Bron, U. König, G. Nénert, *Powder Diffr.* 29 (2014) S13–S18.
- [21] W.C. Oliver, G.M. Pharr, *J. Mater. Res.* 7 (1992) 1564–1583.
- [22] N. Ojala, K. Valtonen, P. Kivikytö-Reponen, P. Vuorinen, V.-T. Kuokkala, *Tribol. - Finnish J. Tribol.* 33 (2015) 36–44.
- [23] V. Ratia, V. Heino, K. Valtonen, M. Vippola, A. Kemppainen, P. Siitonen, V.-T. Kuokkala, *Tribol. - Finnish J. Tribol.* 32 (2014) 3–18.
- [24] H. Hossam, *J. Miner. Mater. Charact. Eng.* 1 (2013) 257–270.

- [25] M. Boccalini Jr., A. Sinatora, in: Proc. 6th Int. Tool. Conf. Karlstadt Univ., 2002, pp. 425–437.
- [26] M. Serna, E.R.B. Jesus, E. Galego, L.G. Martinez, H.P.S. Corrêa, J.L. Rossi, Mater. Sci. Forum 530-531 (2006) 48–52.
- [27] J. Musil, in: Thin Film. Coatings, CRC Press, 2015, pp. 377–464.
- [28] N. Ojala, K. Valtonen, A. Antikainen, A. Kemppainen, J. Minkkinen, O. Oja, V.-T. Kuokkala, Wear (submitted (2016)).
- [29] H. Winkelmann, E. Badisch, M. Roy, H. Danninger, Mater. Corros. 60 (2009) 40–48.
- [30] C. Brett, P. Melo, J. Appl. Electrochem. 27 (1997) 959–964.
- [31] V.A. Alves, C.M.A. Brett, Key Eng. Mater. 230-232 (2002) 436–439.
- [32] V.A. Alves, C.M.A. Brett, Electrochim. Acta 47 (2002) 2081–2091.
- [33] V.A. Alves, C.M.A. Brett, Corros. Sci. 44 (2002) 1949–1965.
- [34] J. Lecomte-Beckers, J. Tchoufang Tchuindjang, E. Pirard, J.-P. Breyer, in: Proc. 14th Roll. Conf. - 1st Conf. Uses Steel, 2002, pp. 507–516.
- [35] V.A. Alves, C.M.A. Brett, A. Cavaleiro, J. Appl. Electrochem. (2001) 65–72.